ASSESSMENT OF FATIGUE BEHAVIOUR OF UHSS STEEL BUTT-WELDED JOINTS BY MEANS OF A FRACTURE MECHANICS METHODOLOGY

C. STEIMBREGER*, N. GUBELJAK**, T. VUHERER**, N. ENZINGER***, W. ERNST****, M. D. CHAPETTI*

**Laboratory of Experimental Mechanics (LABMEX), INTEMA (Institute for Material Science and Technology), CONICET - University of Mar del Plata, J.B. Justo 4302 (B7608FDQ), Mar del Plata, Argentina*
***University of Maribor, Faculty of Mechanical Engineering, Smetanova 17 (2000), Maribor, Slovenia*
****Graz University of Technology, Institute for Materials Science and Welding, Kopernikusg. 24 (8010), Graz, Austria*
*****voestalpine Stahl GmbH, Linz, Austria*

DOI 10.3217/978-3-85125-968-1-26

ABSTRACT

Advances in steel manufacturing technologies made possible the use of high-strength steel (HSS) and ultra-high strength steel (UHSS) in bridges, cranes, offshore structures, oil pipelines and automotive parts. Welding procedures had to be developed to join these materials successfully, but this is still a major issue in mechanical design of HSS elements. Particularly in welding codes and design documents, fatigue resistance of as-welded joints is normally considered to be independent of the base material (BM) static strength. However, cyclic loaded as-welded components with high quality or post-weld treated joints have shown improved performance when using HSS and UHSS as the base material.

The present work aims to apply a fracture mechanics methodology to the analysis of fatigue behaviour of welded joints. The approach requires estimating the driving force available for subcritical crack growth at the location of maximum stress concentration. In this regard, stress intensity factor proved to be a sensible parameter that can account for loading scheme and local weld geometry. It can be determined by numerical modelling, which demands a change from continuum mechanics stress analysis to one that estimates fracture mechanics parameters, considering the existence of defects and cracks. Then, the total driving force applied to the crack can be compared to its threshold for propagation, resulting in the effective driving force for crack growth.

Particularly, the effect of welding process on the fatigue behaviour of ultra-high strength steel butt-welded joints was studied. Sheets of steel S960MC and S960QL were joined with different welding techniques: Gas Metal Arc Welding (GMAW), Laser Hybrid Welding (LHW) and Electron Beam Welding (EBW). To validate the model, fatigue tests were performed with stress ratio R = 0.1, under four points bending loading. Joints manufactured with GMAW exhibited the highest fatigue strength of the three configurations. Compared to the fatigue limit of the BM, a decrease in fatigue strength around 60% was observed in welds jointed with LHW and EBW, although the latter showed longer fatigue lives for higher nominal stresses.

Proposed methodology allows to assess the effect of microstructure, defect size, hardness, and joint geometry resulting from each welding technique. Results conservatively describes the fatigue behaviour of each weld configuration and highlights the relative influence of all factors considered in the assessment. Although the validated results request further studies to improve understanding of the acting

mechanism, they also show the potential of welded HSS and UHSS joints compared to the standard design approaches.

Keywords: Welding process; Welded joints; Ultra-high strength steel; Fracture mechanics approach

NOMENCLATURE

a	crack length
a_f	final crack length
a_i	initial size of defect/initial crack length
$(area)^{1/2}$	square root area parameter
C, m	environmental sensitive material constants
d	microstructural dimension (e.g., grain size)
da/dN	crack propagation rate
HV	Vickers hardness
k	material constant that accounts for development of ΔK_C
N_f	cycles to failure in S-N curves
P	applied load in the four points bending test
R	stress ratio (minimum stress/maximum stress)
s, L	half the minor and major span in four points bending scheme
t	plate thickness
Y	geometrical factor
α	material exponent for R correction
β	weld reinforcement angle
ΔK	applied stress intensity factor range
ΔK_C	"extrinsic" component of ΔK_{th}
ΔK_{dR}	microstructural crack propagation threshold
ΔK_{th}	fatigue crack propagation threshold
ΔK_{thR}	fatigue crack propagation threshold for long cracks
$\Delta\sigma$	nominal applied stress range
$\Delta\sigma_{eR}$	plain fatigue limit (material endurance, dependent on R)
$\Delta\sigma_{th}$	threshold stress range for crack propagation
σ_{UTS}	ultimate tensile strength
σ_{ys}	static yield strength

INTRODUCTION TO THIS DOCUMENT

Among construction materials, high-strength low-alloyed (HSLA) structural steel is particularly attractive due to its satisfactory weldability and high ductility. Immediate applications include structures where the volume of material needed to bear design loads is high, and therefore the weight of metal is comparable to external loads (for example, cranes, long-span beams, and drill string components, among others). At the present time, strength up to 1300 MPa can be found in the market, but this development has not been accompanied accordingly in design codes, as it is usually the case. The former exclusion of HSS and UHSS from documents devoted to welded constructions was due to safety

issues related mainly to the lack of experimental data on these materials in the welded condition, and the uncertainty in their mechanical behaviour. Extensive discussions and well-proved results are needed to achieve a fully developed standard or code dealing with new materials, which justifies this late upgrade in legal documents. This highlights the need for a deep understanding of mechanical response of HSS and UHSS weldments to different loading conditions.

There are currently several methods available to determine fatigue resistance of welded joints, which make use of different stress definitions (nominal stress, structural stress, notch-stress, or hot-spot stress) or, alternatively, employ local strain measurements [1-4]. However, an important aspect in welded joints is that crack initiation period is greatly reduced or suppressed, due to the usual existence of weld flaws and local stress concentrators. Early works on this matter revealed initial crack-like defect depths of about 20-400 μm [5, 6], depending on the welding conditions. In IIW recommendations [1] initial crack lengths in the range of 50 to 150 μm are suggested for fracture mechanics applications. Radaj et al. [4] recommended an initial crack size above $a_i = 100$ μm for life prediction of welded structures. A review by Grover [7] pointed out that even high-quality welds contain flaws up to a depth of about 100 μm. Such defect sizes fall clearly within the short crack regime. This prompted Chapetti et al. to propose in the 2003 annual meeting of the International Institute of Welding [8] (see also reference [9]) a fracture mechanics methodology that employs the resistance curve concept, including the short crack regime, to estimate the fatigue behaviour of welded joints. After this, various studies were performed in order to assess the influence of different mechanical, geometrical and microstructural parameters on the fatigue resistance of welded joints [10-13]. Recently proposed IBESS model [14-16], is also a fracture mechanics methodology, based on the same resistances curve concept that considers the short crack regime. Principal differences arise from methodological aspects and simplification hypothesis, which are out of the scope of the present study. Other assessment techniques can be found in literature (see, for instance, [17] and [18]), but they do not consider the short crack regime and differ in the basic assumptions.

In the present study, a fracture mechanics methodology is described and applied to different butt-welded joints to predict their fatigue behaviour. Three welding processes were considered to join UHSS plates. Fatigue tests were carried out to determine the strength of the welds under constant amplitude loading. Microstructures, hardness, and size of weld defects were measured and used as data input in the assessment.

MATERIALS AND WELDING TECHNIQUES

Materials employed in the present study are structural high-strength low-alloyed steels, designated as S960MC and S960QL in EN 10149-2 [19] and EN 10025-6 [20], respectively. The former is a microalloyed, thermomechanical-processed steel with fine-grained microstructure, consisting principally of martensite and tempered martensite [21, 22]. The second is a hot-rolled, quenched, and tempered steel, with similar microstructure. Steels are supplied in 8 mm thick sheets. Chemical composition is exhibited in Table 1.

Table 1 Chemical composition of steel products, in wt %

Chemical elements	C	Si	Mn	P	∑ (Cr, Ni, Mo)	∑ (V, Nb, Ti)	CEV [23]	CET [23]	P_{CM} [24]
S960MC	0.09	0.12	1.69	0.007	1.63	0.14	0.66	0.34	0.27
S960QL	0.17	0.22	1.23	0.007	0.857	0.05	0.54	0.36	0.3

Butt-welded joints were manufactured with gas metal arc welding (GMAW), laser-hybrid welding (LHW) and electron-beam welding (EBW), with a 2.5 m long weld seam. Weld direction was parallel to the rolling direction. The filler material was BÖHLER alform 960 IG [25], and BÖHLER EMK 8 [26] for GMAW and LHW, respectively. Chemical composition and standard designation of the wires are listed in Table 2. Welding parameters were defined by trial and error [27] with the aim at producing sound and representative welds for each welding process.

Table 2 Chemical composition of steel products, in wt %

Chemical elements	C	Si	Mn	Ni	Cr	Mo	CEV [23]	CET [23]	P_{CM} [24]
G4Si1*	0.1	1.0	1.7	-	-	-	0.38	0.27	0.22
G89 5 Mn4Ni2.5CrMo**	0.12	0.8	1.9	2.35	0.45	0.55	0.79	0.45	0.34

*BÖHLER EMK 8

**BÖHLER alform 960-IG

FRACTURE MECHANICS APPROACH

A fracture mechanics methodology was employed for the fatigue assessment of welded components to analyse different variables of the damaging process. Description of this method and hypothesis needed for its application were thoroughly presented in previous publications from the authors [9-11]. Weld toe geometry, joint design and the presence of undercuts were already studied, and their effect on fatigue strength of weldments could successfully be analysed. This approach is based on the resistance curve concept that compares the total driving force applied to a crack with its threshold for crack propagation. The difference is the energy needed for crack growth, known as the effective driving force.

The applied driving force can be determined as a function of loading configuration (simple traction, bending, or torsion), sample geometry and crack length. To do this, the applied stress intensity factor range, ΔK, has proven to be a proper parameter. Likewise, crack propagation threshold, ΔK_{th}, can be employed to describe crack grow resistance. Both quantities depend on crack size and include the short crack regime. This is particularly useful in the present assessment because of the use of high-strength steels and good quality welds. Relationship between ΔK and ΔK_{th} can be expressed as a modified Paris Law according to Eq. (1).

$$da/dN = C\,(\Delta K - \Delta K_{th})^m \quad (1)$$

where C and m are material constants that depend on the environment. It is important to mention, that in the case of fatigue limit determination, the value adopted by these

constants in Eq. (1) is irrelevant, since for da/dN approaching to zero, the critical stress range is just defined by $\Delta K = \Delta K_{th}$. For higher level of stress, where $\Delta K > \Delta K_{th}$, Eq. (2) must be solved.

$$N_f = \int_{a_i}^{a_f} \frac{da}{C\,(\Delta K - \Delta K_{th})^m} \tag{2}$$

where N_f is the number of cycles needed to grow a crack from initial crack length, a_i, to final crack size, a_f. Both situations described previously can be visualised in Fig. 1a and 1b, for the fatigue strength and the fatigue resistance for finite life estimation, respectively. In the former case, there is a value of $\Delta\sigma$ for which both curves touch at a single point. This is the critical stress or fatigue limit of the configuration, and the contact point between the two curves is the non-propagating crack length. In the second case, the shaded area represents the energy available for fatigue crack growth.

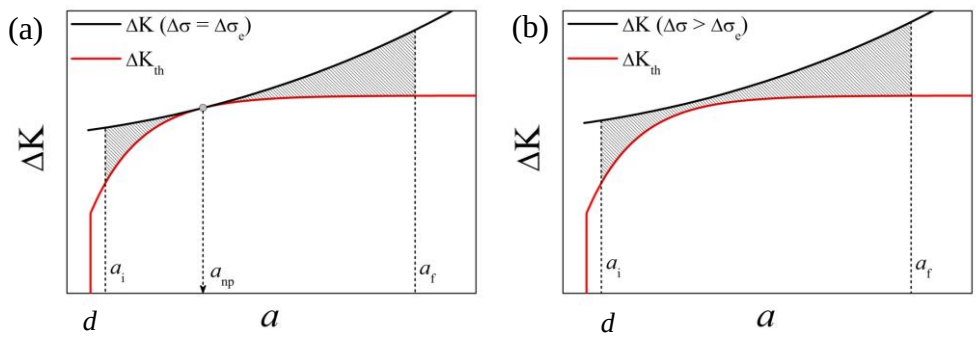

Fig. 1 Graphical method to estimate fatigue resistance of a welded joint for (a) infinite fatigue life (fatigue limit) and (b) finite fatigue life, considering an initial crack length, a_i

To determine the crack propagation threshold, it was suggested [28] that location d of the strongest microstructural barrier defines a microstructural threshold for short crack propagation. This parameter can be expressed as follows:

$$\Delta K_{dR} = Y\,\Delta\sigma_{eR}\,(\pi d)^{1/2} \tag{3}$$

where Y is a geometrical factor and $\Delta\sigma_{eR}$ is the plain fatigue limit, defined as the lowest nominal stress range for crack propagation in a smooth sample. It depends on the stress ratio R, and therefore the microstructural fatigue threshold is also affected by R. The value of microstructural barrier d can be estimated with the ferrite grain size and bainite or martensite lath length [28, 29].

Long crack behaviour is characterised by a constant threshold, represented by ΔK_{thR}, for a given stress ratio R. Difference between this mechanical threshold and microstructural fatigue threshold ΔK_{dR}, is constant and depends on the stress ratio R. However, a transition exists from the short crack behaviour, characterised by ΔK_{dR}, to the long crack regime, where ΔK_{thR} domains crack growth. Chapetti proposed [28] that the development of the extrinsic component ΔK_C can be calculated with Eq. (4).

$$\Delta K_C = (\Delta K_{thR} - \Delta K_{dR})\,\{1 - exp[-k(a-d)]\} \tag{4}$$

where k is a material constant that characterises the transition zone for each stress ratio, and a is the crack length in mm, measured from the free surface.

In summary, the shape of the threshold curve is given by Eq. (5), and it describes the resistance of a material to fatigue crack propagation.

$$\Delta K_{th} = \Delta K_{dR} + \Delta K_C = Y\,\Delta\sigma_{th}\,(\pi a)^{1/2} \tag{5}$$

Replacing Eq. (4) into (5) gives the full form of the threshold curve, as expressed by Eq. (6):

$$\Delta K_{th} = \Delta K_{dR} + (\Delta K_{thR} - \Delta K_{dR})\,\{1 - exp[-k(a-d)]\} \tag{6}$$

which is valid for a ≥ d.

The expression for k is given in Eq. (7). It defines a threshold for fatigue crack propagation that correlates well with experimental data [28].

$$k = \Delta K_{dR} \,/\, [4d\,(\Delta K_{thR} - \Delta K_{dR})] \tag{7}$$

ESTIMATION OF THE APPLIED ΔK. FINITE ELEMENT MODEL

Crack propagation can be quantified by means of a Fracture Mechanics Approach that is extensively described in previous works from the authors [10-13, 28]. In order to apply these methodologies, stress intensity factor range as a function of crack length must be known. With this objective, different finite element (FE) models were conducted, considering representative real weld profiles resulting from each welding procedure. 8 mm plates made of S960MC and S960QL steels were used as the base material and three different welding processes were employed (LHW, EBW and GMAW). Each process gives quite different weld profiles, which results in different crack growth behaviour. These geometries were obtained from cross sections of relevant weld beads, as can be seen in Figs. 2a, 2b and 2c for LHW, EBW and GMAW, respectively. Corresponding weld reinforcement heights and reinforcement angles were 1.08, 0.2 and 0.97 mm, and 144, 150 and 160°, respectively. Average weld toe radius at the crack initiation site was 0.4 mm for LHW and 1.4 mm for GMAW specimens. Because of the presence of undercuts, and crack nucleation from flaw root, toe radius was not determined for EBW samples.

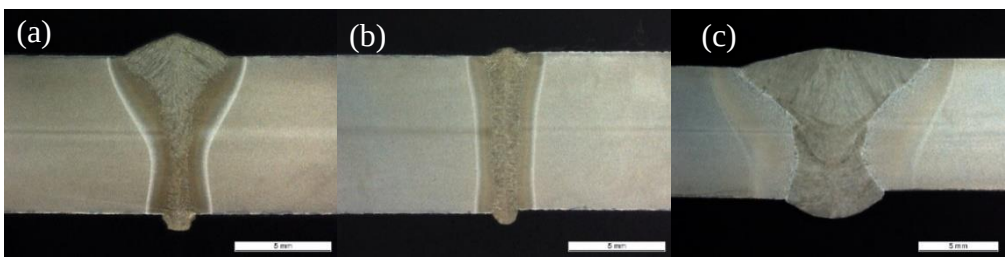

Fig. 2 Weld profile for FEM. (a) LHW (LM). (b) EBW (EM). (c) GMAW (MM)

FE model is depicted in Fig. 3. It consists in a simplified 2D symmetric weld, with a crack, *a*, growing from the weld toe. Four points bending scheme was considered for stress analysis. Minor and major span are represented by *s* and *L*, respectively, *t* is the plate thickness and *P* is the applied load. All these variables define the maximum nominal stress on the surface that is used in S-N curves. Stress intensity factors and real crack path were obtained following software procedure for fracture mechanics simulations [30]. Cracks were introduced as "seam cracks" growing from the weld toe and the maximum energy release criterion was used to determine the crack propagation direction. Concentric circular partitions were done at the crack tip, and the area defined by the first circle was the crack front, which will later be computed as the first contour integral. Mesh at the crack front was constructed with 6-node quadratic plane strain triangles, which use a modified second-order interpolation. The software converts the elements in the crack front to collapsed quadrilateral elements. To improve accuracy, a square root singularity is recommended to be assigned to the crack tip, which constrains the collapsed nodes to move together. 8-node biquadratic plane strain quadrilateral elements were assigned to the rest of the mesh. It must be mentioned that residual stresses and linear or angular misalignment were not considered in this work. Figs. 4a to 4c illustrate examples of mesh configuration and Von Mises (VM) stress distribution close to the crack for LHW, EBW and GMAW, respectively. In all cases, crack length was assumed equal to 0.2 mm and nominal stress equal to the fatigue strength of each weld detail. Note that stresses above 960 MPa are only reached in a very small region around the crack tip.

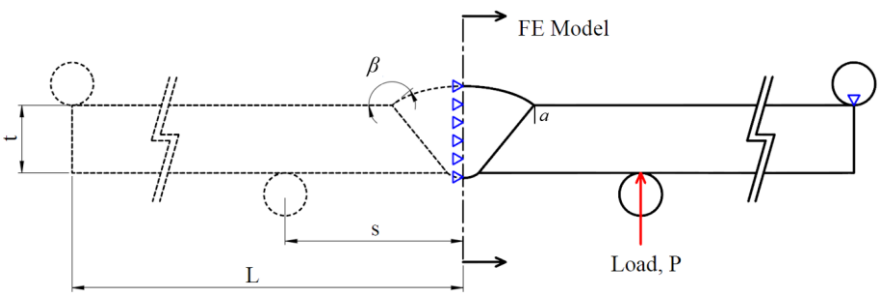

Fig. 3 Geometry, load configuration and boundary conditions of the finite element model. *t* is the plate thickness, *a* is the crack length, β is the reinforcement angle, *s* is half the minor span, *L* is half the major span and *P* is the applied load

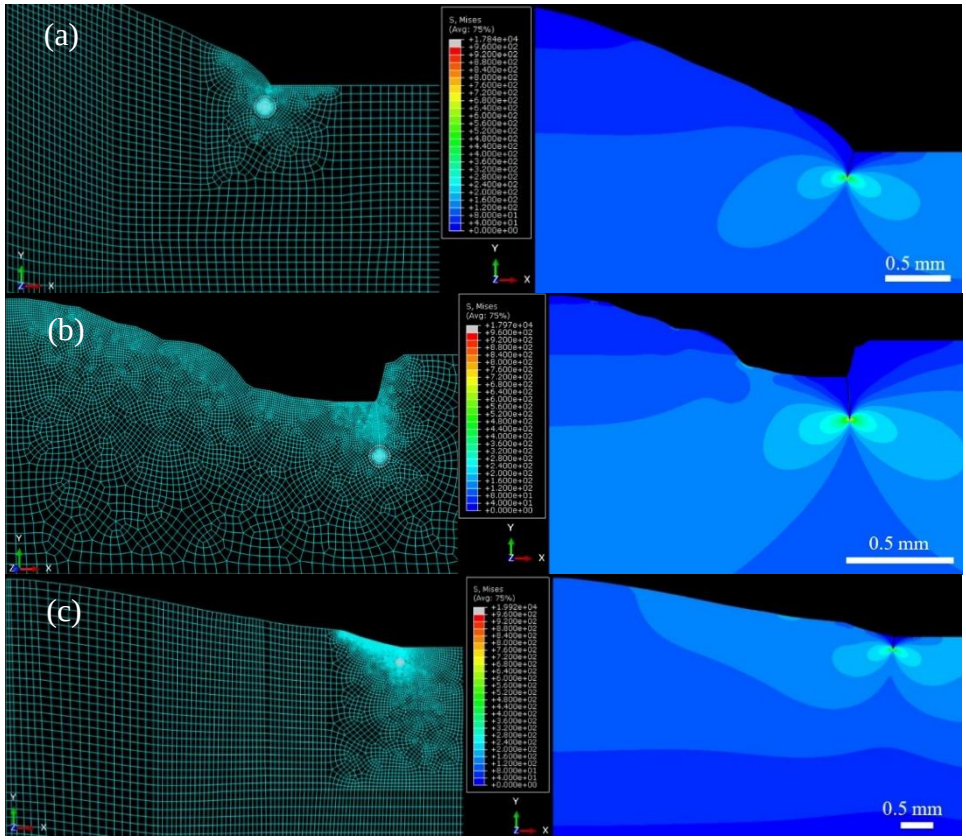

Fig. 4 2D FE mesh and VM stress distribution for a = 0.2 mm and a nominal stress range of 169 MPa. (a) LHW, $\Delta\sigma_{e0.1}$=175 MPa. (b) EBW, $\Delta\sigma_{e0.1}$=189 MPa. (c) GMAW, $\Delta\sigma_{e0.1}$=204 MPa

Stress intensity factor depends on weld geometry, crack length and applied remote stress. Having defined the weld detail and load in the bending test, their values can be obtained for different crack lengths by means of the finite element analysis described previously. This procedure was repeated for different crack lengths ranging from 50 μm to 4 mm, following the path that maximise energy release rate [30]. Step size was varied from 25 μm to 100 μm in the first millimetre, to obtain an accurate profile in the short crack range. For larger crack lengths, 0.5 mm was selected. Fig. 5 presents values of ΔK for different crack lengths. These curves can be plotted together with threshold curve to determine fatigue limit for each case, as it was explained in Fig. 1.

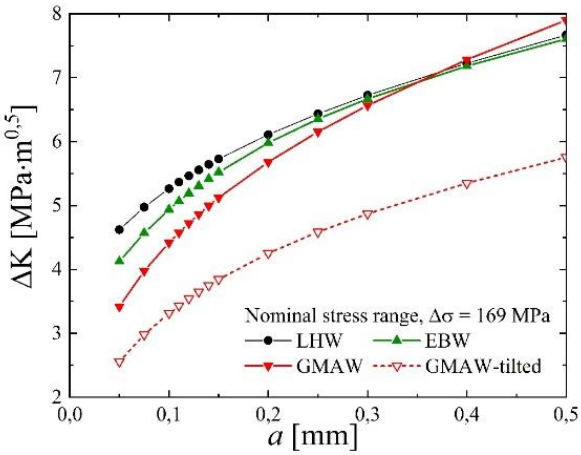

Fig. 5 Stress intensity factor as a function of crack length. Nominal stress range 169 MPa

To explain crack behaviour observed experimentally in some GMAW specimens, where the crack grew following the fusion line, a model was considered using this tilted crack path. Fig. 6a illustrates a side view of a cracked sample, and Figure 6b presents a cross section showing similar tilted profile in early crack growth. FE results for this crack path are shown in Figure 6c, in terms of VM stress. Values of ΔK vs. *a* are also displayed in Fig. 5 (GMAW-tilted).

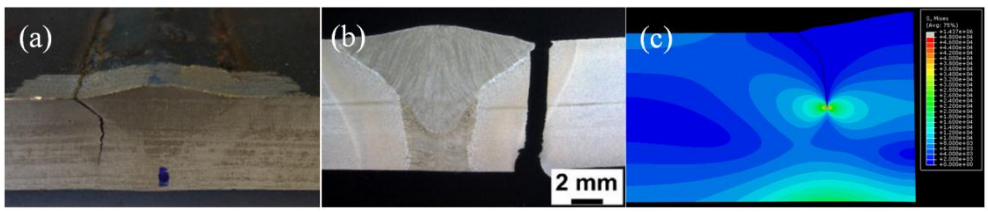

Fig. 6 (a) Fatigue crack path at the side of the sample. (b) Cross section showing early crack grow following the fusion line. (c) FE results in terms of VM stress. Nominal stress range: 169 MPa

THRESHOLD CURVE DETERMINATION

Threshold curve can be determined by means of several parameters and mechanical properties, defined for the microstructure developed in the crack initiation zone, preferably. In the following, each variable is considered and discussed separately.

Strongest microstructural barrier, d

In the 80´s and 90´s microstructure and grain boundaries and their relation with plain fatigue limit were deeply studied [29, 31-37]. It was found that the fatigue limit of plain and blunt-notched specimens in steels is defined by the ability of the strongest microstructural barrier, *d*, to arrest a small crack. For engineer applications, *d* can be related to a microstructural characteristic dimension, such as ferrite grain size and bainite or martensite lath length [28, 29, 32]. In the present work, microstructure was analysed in the crack initiation zone, and an average local grain size was determined. Since all cracks nucleated preferably in the CG-HAZ, variation of grain size was not significant. Therefore, d = 30 μm will be assumed for all welds.

Intrinsic fatigue threshold in the resistance curve is also affected by *d* according to Eq. (3). It additionally modifies the development of the extrinsic component as shown in Eq. (7). Bigger grain sizes lead to higher values of ΔK_{dR}, and a retarded development of the plateau in the threshold curve. The overall effect on the fatigue strength of the weld will be determined together with the applied driving force for crack propagation.

Due to the fact that cracks usually form with a semi-circular shape, the geometrical factor *Y* in Eq. (3) can be assumed to be 0.65 [38, 39].

Intrinsic fatigue threshold, ΔK_{dR}

In the present methodology, the plain fatigue limit refers to the resistance of material to fatigue cracking in conventional fatigue testing. $\Delta\sigma_{eR}$ is 550 MPa at R = 0.1 for test performed in steel S960MC under traction loading mode. Fatigue limit for bending may be different [13, 40-42]. This must be considered a first approach, since cracks may nucleate in a microstructure different from that of the BM. There are two options to take this into account in assessment. First, an empirical correlation can be used to determine $\Delta\sigma_{eR}$ as a function of hardness or tensile strength, considering proportionality with fatigue strength [43]. In the former case, relationship can be written as presented in Eq. (8), which should later be used in Eq. (3) to obtain ΔK_{dR}.

$$\Delta\sigma_{eR}\ (BM)\ /\ \Delta\sigma_{eR}\ \ (HAZ)\ =\ HV\ (BM)\ /\ HV\ (HAZ) \tag{8}$$

Second, ΔK_{dR} can be estimated using the Murakami-Endo model, expressed as shown in Eq. (9).

$$\Delta K_{dR}\ =\ 0.0033\ (HV + 120)\left(\sqrt{area}\right)^{1/3}\ \left[\frac{1-R}{2}\right]^{\alpha} \tag{9}$$

where $\alpha = 0.266 + HV \cdot 10^{-4}$ and $\sqrt{area}$ refers to the square root of defect/crack area projected normal to the maximum principal stress, according to Murakami´s proposal [43]. Eq. (9) can be expressed in terms of the average grain size, *d*, as follows [44]:

$$\Delta K_{dR} = 0.00356\ (HV + 120) d^{1/3}\ \left[\frac{1-R}{2}\right]^{\alpha} \tag{10}$$

with ΔK_{dR} in MPa·m$^{1/2}$, for *d* in μm and HV in kgf/mm^2.

Steel S960MC and S960QL have an average hardness of 320 and 350 $HV_{0.5}$, respectively. Depending on the welding process and filler materials different hardness

values are achieved in the HAZ. Measured values were in accordance with results from microstructures simulated by Gleeble. These outcomes are displayed in Table 3. Additionally, last column presents values of microstructural fatigue threshold, ΔK_{dR}, as estimated with Eqs. (3) and (8), and (10), using Gleeble hardness and d = 30 μm for all welds. Fatigue strength of S960QL had to be estimated using fatigue strength of S960MC and Eq. (8).

Table 3 Mechanical properties and important parameters for the model. R = 0.1.

		d [μm]	HV_{10} (Gleeble)	$\Delta\sigma_{eR}$ [MPa]	ΔK_{dR} [MPa√m]	
Base Material	**Welding Process**	**HAZ**	**1200°C**	**BM**	**Eqs. (3) and (8)**	**Eq. (10)**
S960MC	LHW	30	350	550	3.80	4.09
	EBW		370		4.01	4.26
	GMAW		330		3.58	3.92
S960QL	LHW	30	420	600	4.55	4.67
	EBW		420		4.55	4.67
	GMAW		390		4.23	4.42

Long crack propagation threshold, ΔK_{thR}

Although long crack propagation threshold was determined experimentally, reproducible values were only obtained for BM, giving 7.38 ± 0.22 and 8.5 MPa√m for S960MC and QL, respectively. It is expected a lower threshold for harder microstructures, as it was found in several investigations [45, 46]. Particularly, Eq. (11) expresses the relationship between long crack propagation threshold and ultimate tensile strength [46]. Additionally, the latter can be estimated with hardness measurements according to Eq. (12). Outcomes are presented in Table 4. In this sense, it can be seen in Figs. 4 and 6 that cracks grew preferably throughout the HAZ, thus justifying the use of a smaller ΔK_{thR} than that of the BM.

$$\Delta K_{th0.1} = -0.0021\,\sigma_{UTS} + 8.4 \tag{11}$$

$$\sigma_{UTS} = 3.26\,HV \tag{12}$$

It must be highlighted that the higher the ΔK_{thR}, the wider the range of crack length covering the development of the extrinsic threshold.

Table 4 Mechanical properties and important parameters for the model. R = 0.1. Values of C for ΔK in MPa·m^{0,5} and da/dN in m/cycle.

	σ_{ys} [MPa]	σ_{UTS} [MPa]	ΔK_{thR} [MPa√m]			C [mm/cycle]	m
Zone	BM	BM	BM		HAZ	BM	BM
S960MC	988	1014	7.38	LHW	6.0 (350 HV)	1.64E-7 – 1.73E-6	2.08 ± 0.34
				EBW	5.87 (370 HV)		
				GMAW	6.14 (330 HV)		
S960QL	963	1043	8.5	LHW	5.52 (420 HV)	5.5E-7	2
				EBW	5.52 (420 HV)		
				GMAW	5.73 (390 HV)		

Paris equation constants, C and m

Like ΔK_{thR}, C and m can be obtained from experimental tests. Results are also displayed in Table 4 for base metals. Although some tests were performed for microstructures different from the base material, more outcomes are needed to assess experimental scatter, which can be large in this kind of test. In this regard, it is important to mention that a statistical determination of C and m can be done, and it may lead to better estimations of the finite life regime. The fracture mechanics model can consider these variations based on Eq. (1). For the present assessment, the lower experimental value of C was considered (1.64E-7) and the average value of m =2.08 will be used (for ΔK in MPa·m^{0,5} and da/dN in mm/cycle), which are similar to those obtained by Lukács for a welded joint made of steel S960MC [47].

Initial crack length, a_i

IIW recommendations [1] define an initial crack length for fracture mechanics assessment of welded joints between 50 and 150 μm. Based on the work from Signes [5] and Watkinson [6], BS 7910 recommends values from 100 to 250 μm. In the present work, an initial crack length of 100 μm can be assumed for LHW and EBW, according to fracture surface inspection. In contrast, GMAW resulted in better quality toe profiles. Therefore, a slightly lower crack length of 50 μm can be considered. Both values fall within the typical ranges from literature.

FATIGUE STRENGTH DETERMINATION

Having calculated ΔK vs. a for a predefined Δσ and a propagation threshold curve, ΔK_{th}, fatigue strength can be determined by solving Eq. (2) for every stress level (above fatigue endurance). a_f was defined as $t/2$ [1, 4] for the present analysis, where t = 8 mm. Results can be appreciated in Figs. 7a and 7b, for S960MC and S960QL, respectively. Since Murakami´s modified equation in Eq. (10) is well-known and widespread, fatigue estimations were calculated using the value of ΔK_{dR} resulting from this expression.

Fatigue strength did not show significant differences when modifying the BM. LHW specimens resulted in 175 MPa and 176 MPa for S960MC and S960QL, respectively. EBW presented higher resistance to fatigue cracking, with a fatigue strength of 189 and 188 MPa for S960MC and S960QL, respectively. Finally, stronger welds were obtained with GMAW process, giving 222 and 246 MPa for respective steels and smaller initial crack size a_i = 50 μm.

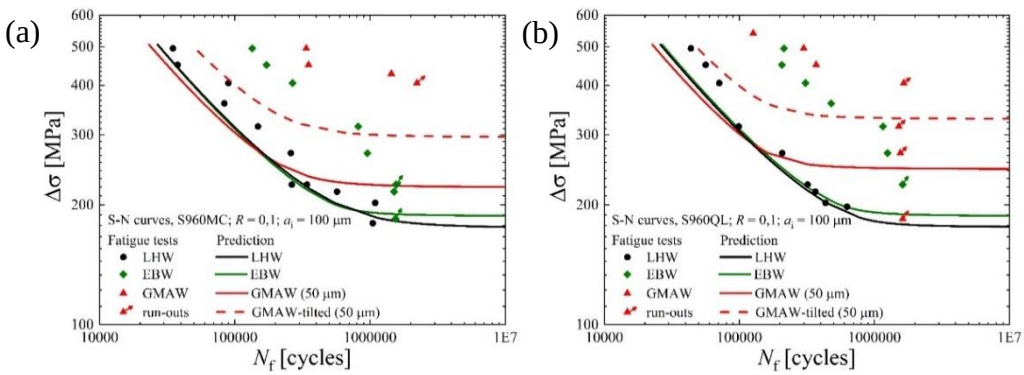

Fig. 7 S-N curves with fatigue strength predictions for (a) S960MC and (b) S960QL

DISCUSSIONS

In the present work two base materials (S960MC and S960QL) were welded with three different welding processes (LHW, EBW and GMAW). Sound welds were obtained with proper selection of welding parameters, and fatigue tests were carried out considering four points bending configuration. S-N curves for weld toe failure are shown in Fig. 7 and reproduced in Fig. 8 for all combinations of welding procedure and base metal. No relevant differences between S960MC and S960QL welds were found. However, a notable reduction in fatigue strength around 60% could be observed in LHW joints compared to BM S960MC. EBW unions showed slightly higher fatigue resistance than their counterpart, and longer fatigue lives for higher nominal stresses. Joints manufactured with GMAW presented the highest fatigue strength, with a ca. 20% decrease compared to standard specimens made of S960MC. Moreover, slope is similar to that of the base material. These results confirm the detrimental effect of fusion welding processes on fatigue performance. However, differences between the three welding methods were not expected to be large, since they are all butt-welds tested under the same loading configuration. IIW recommendations [1] set a maximum fatigue strength of FAT 90 for a butt joint with reinforcement, at 2 million cycles with 95% probability of survival in the as welded conditions. If a thinness effect [1] is considered for the 8 mm thick plate, a higher strength of FAT 113 is obtained. This curve is presented in Fig. 8 with a slope m = 3, laying below all experimental points. LHW results suit well to this FAT value, but it is conservative for EBW and GMAW joints. In these cases, fatigue resistance is even higher than recommendation of FAT 140 for a transversely loaded butt-weld ground flush

to plate, corrected by thickness effect (FAT 112·(25/8)^0.2=FAT 140). Best FAT curves for EBW and GMAW are displayed, showing that a FAT 200 with a slope of 3.5 and a FAT 300 with a slope of 5 are respectively suitable. These high fatigue strengths and changes in slopes were also observed in high-performing welds [40, 47-49] and post weld treated joints [17, 50-52].

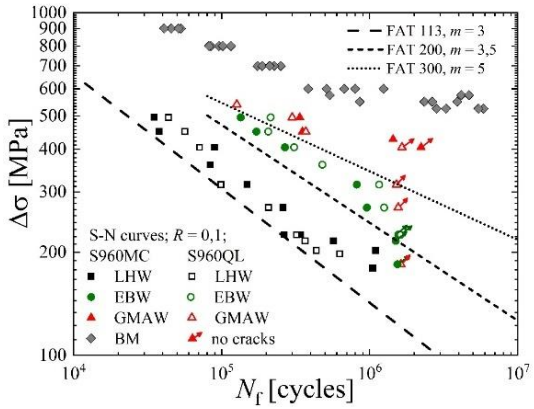

Fig. 8 Nominal stress range vs. cycles to failure, with standard FAT curves from IIW [4]

To analyse these variations in fatigue behaviour, a fracture mechanics methodology was applied to cracks growing from weld toes. Thorough experimental measurements were made to obtain input data for the model, although some parameters had to be estimated using hardness results. This approach is different from other fatigue life estimation techniques, like the hot-spot or the notch stress approach [3], because it considers an initial crack size, disregarding the crack initiation stage. This allows to predict fatigue strengths if the short crack behaviour is included [29, 32, 33-37].

Relevant weld profiles were simulated in a finite element model, to obtain stress intensity factors for cracks growing from the weld toe. Fatigue threshold was determined using a microstructural dimension, d, of 30 μm and a long crack propagation threshold defined by local hardness measurements. Fatigue strengths were calculated for a_i = 100 μm in LHW and EBW samples, and for a_i = 50 μm in GMAW specimens. This is justified because the latter resulted in high quality welds, with smooth weld profile and no remarkable flaws at the initiation site. Results agreed with fatigue tests, giving the highest strength for GMAW batch, although prediction was still very conservative. In the finite life regime, predictions were also conservative for EBW and GMAW specimens, but slightly unconservative for LHW. As it was mentioned previously, fracture mechanics methodology can consider variations of C that may results from experimental testing. More accurate determinations of constants in Eq. (1) might definitely lead to better predictions in the finite life region. Furthermore, a statistical analysis of each variable that serves as input data for the model is feasible. This will give confident bands for predicted S-N curves.

In the case of GMAW specimens, a tilted crack path was observed during early propagation, as depicted in Fig. 16. From an energetic point of view, this is not the most

critical situation, and therefore it is expected a reduction in the stress intensity factor along the new crack path. It can be thought that some metallurgical factors (for instance, fusion line and CG-HAZ) are contributing to early crack growth, deviating crack path from what it would be, according to stress configuration. When considering the deviated initiation, a higher less-conservative fatigue strength was obtained, although predictions could not precisely reproduce the experimental endurance observed in GMAW samples. Further studies are needed to better predict these specimens' behaviour.

In summary, conservative predictions of fatigue strength were obtained for all welding processes. Results highlight the ability of fracture mechanics methodologies to safely predict the fatigue behaviour of welded components. Several contributing factors were considered, and their effects could be quantified. This is very attractive from a design point of view, but also, for developing less conservative but safe standards and construction codes. Additionally, enhanced fatigue strength observed in high quality welds and post-weld treated joints made of high strength and ultra-high strength steels, can be assessed. In the former case, fewer defects reduce initial crack length, which is translated into a higher strength as it was the case for GMAW samples. Although this could not completely explain the superior fatigue strength of GMAW specimens, it demonstrates the ability of the fracture mechanics approaches to reproduce variation in endurances when relevant parameters are changed. On the other hand, TIG-dressing not only re-shape weld profile, but also introduce residual stresses [53]. In this regard, much effort is needed to adequately include residual stresses in the analysis, which is subject of a future publication from the authors.

CONCLUSIONS

The development of fracture mechanics methodologies that include short crack behaviour made it possible to estimate fatigue lives and fatigue limits of welded joints. The suppression or reduction of the crack initiation stage allows to consider solely crack propagation in the assessment of each weld detail, with reasonable accuracy. Additionally, the resistance curve concept is employed to relate the driving force for crack propagation with material´s resistance. Determination of the latter is the main difference between models currently available for this kind of assessment. In this work, Chapetti´s model was used to calculate the threshold curve. This method demands experimental measurement of some mechanical parameters, such as grain size, hardness, and plain fatigue limit, at the crack initiation region. For welds, this can be the WM, the HAZ or the BM.

In the present study, three different welding processes were used to join 8 mm thick plates made of steels S960MC and S960QL. Dog-bone samples were machined from the main plate in all configurations to obtain S-N curves under four points bending scheme. Weld geometry, microstructure, hardness, and weld defects were evaluated close to the weld toe, where all samples failed. Experimental outcomes were used in the fracture mechanics methodology, which was applied to all combinations of welding processes and base materials. Results conservatively describe the fatigue behaviour of each configuration and highlight the relative influence of all factors considered in the assessment. Weld profile cannot solely explain the differences between S-N curves

because there is also an influence of weld defects (undercuts and underfills) on early crack propagation, particularly for LHW and EBW. GMAW samples resulted in the highest fatigue resistance, which reflects the benefits that can be experienced when using HSS or UHSS as BMs. In this regard, welds made with GMAW showed high quality profile, which can be translated into a smaller initial crack length in the fracture mechanics approach that enhances the fatigue strength. This, however, cannot reproduce by itself the superior endurance observed in GMAW specimens. Additionally, some metallurgical effects may have contributed to early crack propagation, giving a tilted crack with a lower stress intensity factor along crack path.

Although residual stresses were not considered in this work, the methodology is able to describe their effect on fatigue behaviour, which is subject of a future work from the authors. Finally, it must be pointed out that accuracy of estimations is better, the better the determination of relevant parameters. In this sense, statistical studies can be performed to obtain ranges of fatigue endurances and fatigue lives for different weld configurations.

ACKNOWLEDGEMENTS

Authors wish to express their gratitude to the funding provided by Agencia Nacional de Promoción Científica Tecnológica, Argentina (PICT 2017 Nro.0982). Support was also provided by the K-Project Network of Excellence for Metal JOINing which is fostered in the frame of COMET - Competence Centers for Excellent Technologies by BMWFW, BMVIT, FFG, Land Oberösterreich, Land Steiermark, Land Tirol and SFG. The programme COMET is handled by FFG. Additionally, the authors would like to acknowledge the Slovenian Research Agency (ARRS) for financial support of the Research Program P2-0137 “Numerical and experimental analysis of mechanical systems”.

References

[1] A. F. HOBBACHER: *Recommendations for Fatigue Design of Welded Joints and Components*, 2nd ed., Springer International Publishing, 2016.

[2] British Standard, BS 7608-2014: *Guide to fatigue design and assessment of steel products*, BSI Standards Limited, 2014.

[3] D. RADAJ: *Design and analysis of fatigue resistant welded structures*, Abington Publishing, 1990.

[4] D. RADAJ, C. M. SONSINO and W. FRICKE: *Fatigue assessment of welded joints by local approaches*, 2nd edition, Woodhead publishing limited, Cambridge, England, 2006.

[5] E. G. SIGNES: ‘Factors affecting the fatigue strength of welded high strength’, *Brit. J.*, 14, 108-116, 1967.

[6] F. WATKINSON, P. H. BODGER, J. D. HARRISON: ‘The fatigue strength of welded joints in high strength steel and methods for its improvement’, *Int conference on fatigue welded structures*, The WI, 97, 1970.

[7] J. L. GROVER: ‘Initial flaw size estimating procedures for fatigue crack growth calculations’, *Int conference on fatigue of welded construction*, Brighton, vol. 275, 1987.

[8] M. D. CHAPETTI, J. BELMONTE, T. TAGAWA, T. MIYATA: ‘On the influence of short crack behaviour on fatigue strength of welded joints’, *IIW X-1545-03 XIII-1971-03*, 2003.

[9] M. D. CHAPETTI, J. BELMONTE, T. TAGAWA and T. MIYATA: 'Integrated fracture mechanics approach to analyse fatigue behaviour of welded joints', *Sci tech weld join*, 9(5), 430-438, 2004.
[10] M. D. CHAPETTI and L. F. JAUREGUIZAHAR: 'Fatigue behavior prediction of welded joints by using an integrated fracture mechanics approach', *International Journal of Fatigue*, 43, 43-53, 2012.
[11] C. STEIMBREGER and M. D. CHAPETTI: 'Fatigue strength assessment of butt-welded joints with undercuts', *International Journal of Fatigue*, 105, 296-304, 2017.
[12] C. STEIMBREGER, N. GUBELJAK, N. ENZINGER, W. ERNST and M. D. CHAPETTI: 'Influence of static strength on the fatigue resistance of welds', *In MATEC Web of Conf* (Vol. 165, p. 13010), EDP Sciences, 2018.
[13] C. STEIMBREGER and M. D. CHAPETTI: 'Fracture mechanics based prediction of undercut tolerances in industry', *Engineering Fracture Mechanics*, 211, 32-46, 2019.
[14] M. MADIA, U. ZERBST, H. T. BEIER and B. SCHORK: 'The IBESS model–Elements, realisation and validation', *Engineering Fracture Mechanics*, 198, 171-208, 2018.
[15] U. ZERBST, M. MADIA, B. SCHORK, J. HENSEL, P. KUCHARCZYK, D. TCHOFFO NGOULA, ET AL.: *Fatigue and fracture of weldments. The IBESS approach for the determination of the fatigue life and strength of Weldments by fracture mechanics analysis*, Switzerland, Springer, 2019c.
[16] U. ZERBST and J. HENSEL: 'Application of fracture mechanics to weld fatigue', *International Journal of Fatigue*, 139, 105801, 2020.
[17] R. RANJAN, S. WALBRIDGE: '2D fracture mechanics analysis of HFMI treatment effects on the fatigue behaviour of structural steel welds', *Welding in the World*, 65(9), 1805-1819, 2021.
[18] R. GOYAL and G. GLINKA: 'Fracture mechanics-based estimation of fatigue lives of welded joints', *Welding in the World*, 57(5), 625-634, 2013.
[19] DIN EN 10149-2: *Hot rolled flat products made of high yield strength steels for cold forming - Part 2: Technical delivery conditions for thermomechanically rolled steels*, Deutsches Institut fuer Normung E.V., 2013.
[20] DIN EN 10025-6: *Hot rolled products of structural steels - Part 6: Technical delivery conditions for flat products of high yield strength structural steels in the quenched and tempered condition*, Deutsches Institut fuer Normung E.V., 2020.
[21] C. SCHNEIDER, W. ERNST, R. SCHNITZER, H. STAUFER, R. VALLANT and N. ENZINGER: 'Welding of S960MC with undermatching filler material', *Welding in the World*, 62(4), 801-809, 2018.
[22] M. PRANGER: *Vergleich der Mikrostruktur ausgewählter hochfester Schweißungen*, Diplomarbeit, K-Projektes Network of Excellence for Metal JOINing (JOIN), Montanuniversität Leoben, 2017.
[23] DIN EN 1011-2:2001-05: *Welding - Recommendation for welding of metallic materials - Part 2: Arc welding of ferritic steels*, Deutsches Institut fuer Normung E.V., 2001.
[24] AWS D1.1/D1.1M:2015: *Structural Welding Code – Steel*, American Welding Society, 23rd ed. USA, 2015.
[25] BÖHLER alform 960 IG datasheet.
[26] BÖHLER EMK 8 datasheet.
[27] C. SCHNEIDER: *Influence of high energy density fusion welding techniques on welding of structural steel S960*, PhD Thesis, TU Graz, 2020.
[28] M. D. CHAPETTI: 'Fatigue propagation threshold of short cracks under constant amplitude loading', *International Journal of Fatigue*, 25(12), 1319-1326, 2003.
[29] K. J. MILLER: 'The two thresholds of fatigue behaviour', *Fatigue & Fracture of Engineering Materials & Structures*, 16(9), 931-939, 1993.
[30] Dassault Systèmes, Simulia: *Abaqus 6.13 User manual*, Providence, RI, USA, 2013.

[31] D. TAYLOR and J. F. KNOTT: 'Fatigue crack propagation behaviour of short cracks; the effect of microstructure', *Fatigue & Fracture of Engineering Materials & Structures*, 4(2), 147-155, 1981.
[32] J. LANKFORD: 'The influence of microstructure on the growth of small fatigue cracks', *Fatigue & Fracture of Engineering Materials & Structures*, 8(2), 161-175, 1985.
[33] M. D. CHAPETTI, T. KITANO, T. TAGAWA and T. MIYATA: 'Fatigue limit of blunt-notched components', *Fatigue & fracture of engineering materials & structures*, 21(12), 1525-1536, 1998.
[34] K. TANAKA and Y. AKINIWA: 'Resistance-curve method for predicting propagation threshold of short fatigue cracks at notches', *Engineering Fracture Mechanics*, 30(6), 863-876, 1988.
[35] A. J. MCEVILY and K. MINAKAWA: 'On crack closure and the notch size effect in fatigue', *Engineering fracture mechanics*, 28(5-6), 519-527, 1987.
[36] M. H. EL HADDAD, T. H. TOPPER and K. N. SMITH: 'Prediction of non propagating cracks', *Engineering fracture mechanics*, 11(3), 573-584, 1979.
[37] J. R. YATES and M. W. BROWN: 'Prediction of the length of non-propagating fatigue cracks', *Fatigue & Fracture of Engineering Materials & Structures*, 10(3), 187-201, 1987.
[38] T. R. GURNEY: *Fatigue of welded structures*, 2nd ed., London: Cambridge UP, 1979.
[39] S. J. MADDOX: *Fatigue strength of welded structures*, 2nd ed., Abington, Cambridge, 1991.
[40] R. J. M. PIJPERS: *Fatigue strength of welded connections made of very high strength cast and rolled steels*, PhD Thesis, TU Delft, 2011.
[41] A. ESIN: 'A method for correlating different types of fatigue curve', *International Journal of Fatigue*, 2(4), 153-158, 1980.
[42] H. ÖZDEŞ, M. TIRYAKIOĞLU and P. D. EASON: 'On estimating axial high cycle fatigue behavior by rotating beam fatigue testing: Application to A356 aluminum alloy castings', *Materials Science and Engineering: A*, 697, 95-100, 2017.
[43] MURAKAMI: *Metal Fatigue-Effects of small defects and non-metallic inclusions*, Elsevier, 2002.
[44] M. D. CHAPETTI: 'Fracture mechanics for fatigue design of metallic components and small defect assessment', *International Journal of Fatigue*, 154, 106550, 2022.
[45] D. TAYLOR: *Fatigue thresholds*, London: Butterworth & Co., 1989.
[46] M. D. CHAPETTI: 'A simple model to predict the very high cycle fatigue resistance of steels', *International Journal of Fatigue*, 33(7), 833-841, 2011.
[47] J. LUKÁCS: 'Fatigue crack propagation limit curves for high strength steels based on two-stage relationship', *Engineering Failure Analysis*, 103, 431-442, 2019.
[48] H. REMES, P. GALLO, J. JELOVICA, J. ROMANOFF and P. LEHTO: 'Fatigue strength modelling of high-performing welded joints', *International Journal of Fatigue*, 135, 105555, 2020.
[49] I. LILLEMÄE, H. REMES, S. LIINALAMPI and A. ITÄVUO: 'Influence of weld quality on the fatigue strength of thin normal and high strength steel butt joints', *Welding in the World*, 60(4), 731-740, 2016.
[50] A. AHOLA, A. MUIKKU, M. BRAUN and T. BJÖRK: 'Fatigue strength assessment of ground fillet-welded joints using 4R method', *International journal of fatigue*, 142, 105916, 2021.
[51] M. LEITNER and M. STOSCHKA: 'Effect of load stress ratio on nominal and effective notch fatigue strength assessment of HFMI-treated high-strength steel cover plates', *International Journal of Fatigue*, 139, 105784, 2020.
[52] R. RANJAN, S. WALBRIDGE: '2D fracture mechanics analysis of HFMI treatment effects on the fatigue behaviour of structural steel welds', *Welding in the World*, 65(9), 1805-1819, 2021.
[53] H. METTÄNEN, T. NYKÄNEN, T. SKRIKO, A. AHOLA and T. BJÖRK: 'Fatigue strength assessment of TIG-dressed ultra-high-strength steel fillet weld joints using the 4R method', *International Journal of Fatigue*, 139, 105745, 2020.